# Ab Initio Calculation of the Photoelectron Spectra of the Hydroxycarbene Diradicals

**Lucas Koziol,[†] Vadim A. Mozhayskiy,[†] Bastiaan J. Braams,[‡] Joel M. Bowman,[‡] and Anna I. Krylov*,[†]**

*Department of Chemistry, University of Southern California, Los Angeles, California 90089-0482, C. L. Emerson Center for Scientific Computation, Department of Chemistry, Emory University, Atlanta, Georgia 30322*

*Received: April 15, 2009; Revised Manuscript Received: May 19, 2009*

Photoelectron spectra of the cis and trans isomers of HCOH were computed using vibrational wave functions calculated by diagonalizing the Watson Hamiltonian, including up to four mode couplings. The full-dimensional CCSD(T)/cc-pVTZ potential energy surfaces were employed in the calculation. Photoionization induces significant changes in equilibrium structures, which results in long progressions in the $\nu_5$, $\nu_4$, and $\nu_3$ modes. The two isomers show progressions in different modes, which leads to qualitatively distinguishable spectra. The spectra were also calculated in the double harmonic parallel-mode (i.e, neglecting Duschinsky rotation) approximation. Calculating displacements along the normal coordinates of the cation state was found to give a better approximation to the vibrational configuration interaction spectrum; this is due to the effects of Duschinsky rotations on the vibrational wave functions.



## I. Introduction

Hydroxycarbene, HCOH, is a high-energy diradicaloid isomer of formaldehyde. It is believed to play a role in formaldehyde photochemistry and its "roaming hydrogen" dynamics, the interstellar medium, and reactions of carbon atom with water.[1−5] HCOH production is a major channel in the photodissociation of hydroxymethyl radical, $CH_2OH$, in the 3p Rydberg state.[6] Reisler and co-workers determined the heat of formation of the deuterated isotope HCOD to be $24 \pm 2$ kcal/mol.[7] Recently, its synthesis and spectroscopic characterization were reported by Schreiner et al.,[8] who isolated the *trans*-HCOH and HCOD in argon matrix at 11 K and identified several infrared (IR) band origins. The experiment was supported by variational calculations of the anharmonic energies using the CCSD(T)/cc-pVQZ quartic force field. In an independent study, the vibrational levels and IR intensities for the ground states of neutral *cis*- and *trans*-HCOH were reported.[9] The calculated lines and intensities matched the experimental data of Schreiner et al. closely. It was found that anharmonicities were crucial for correctly describing IR intensities as well as energies. The harmonic approximation described the lowest fundamental frequencies accurately, although it overestimated the stretching modes by approximately 200 $cm^{-1}$ in both isomers. Several combination/overtone bands acquired intensity in the low-energy region ($0-3000$ $cm^{-1}$) and complicated the spectrum.

The cation $HCOH^+$ has also been studied. Berkowitz[10] and also Burgers[11] observed the species by mass spectroscopy in the dissociative photoionization of methanol. Near the dissociation threshold of hydrogen elimination, $HCOH^+$, rather than $H_2CO^+$, was the dominant product.[10] Radom and co-workers characterized *trans*-$HCOH^+$, formaldehyde cation, and the transition state using molecular orbital theory.[12] They were the first to suggest that $HCOH^+$ is the most stable isomer of ionized formaldehyde. The following year, McLafferty and co-workers[13] performed collision-activated mass spectroscopy experiments and were able to infer the stability of a product in the correct energy range, which they attributed to $HCOH^+$. The heat of formation, based on careful comparison between theoretical calculations and experimental data (reverse activation energy and isotope effects were found to be crucial in analysis of appearance energy experiments) was established by Radom and co-workers.[14] The energy difference between the formaldehyde cation and $HCOH^+$ was found to be poorly reproduced by perturbation theory (MP2) due to convergence issues in the perturbative series. Finally, Wiest[15] characterized energy and structure for both cis and trans isomers in a DFT study of the methanol radical cation surface.

Neutral HCOH tunnels effectively through the barrier to formaldehyde.[8] The calculated rate constant for the forward reaction is almost an order of magnitude higher than for the reverse reaction,[16] as would be expected from energetics. Whereas on the neutral surface, HCOH is much higher than formaldehyde, the energy gap between $HCOH^+$ and $H_2CO^+$ is much smaller (1811 $cm^{-1}$; see Figure 1). Thus, it might be easier to observe HCOH isomer in the ionized rather than neutral state.

From the electronic structure point of view, HCOH is an example of substituted carbenes, diradical species playing an important role in organic chemistry.[17] Spectroscopically, prototypical substituted carbenes have been studied by Reid and co-workers.[18−21] Using high-resolution spectroscopy, they characterized the singlet−triplet gaps, spin−orbit couplings, and mode-specific dynamics of several triatomic carbenes.[18−21] Halogen substitution reduces diradical character, resulting in the singlet ground state. The OH group has a similar effect: the ground state of hydroxycarbene is a singlet, and the singlet−triplet gap is about 1 eV.[2−5,22,23]

In this work, we calculate the vibrational levels of ground-state $HCOH^+$ and the associated photoelectron spectra from ground vibrational states of *cis*- and *trans*-HCOH. Photoelectron spectroscopy is a sensitive tool that provides information about electronic structure and nuclear motion. Positions of band heads yield ionization energies (IEs) and an electronic spectrum of

* Corresponding author. E-mail: krylov@usc.edu.
[†] University of Southern California.
[‡] Emory University.

10.1021/jp903476w CCC: $40.75 
Published on Web 06/17/2009

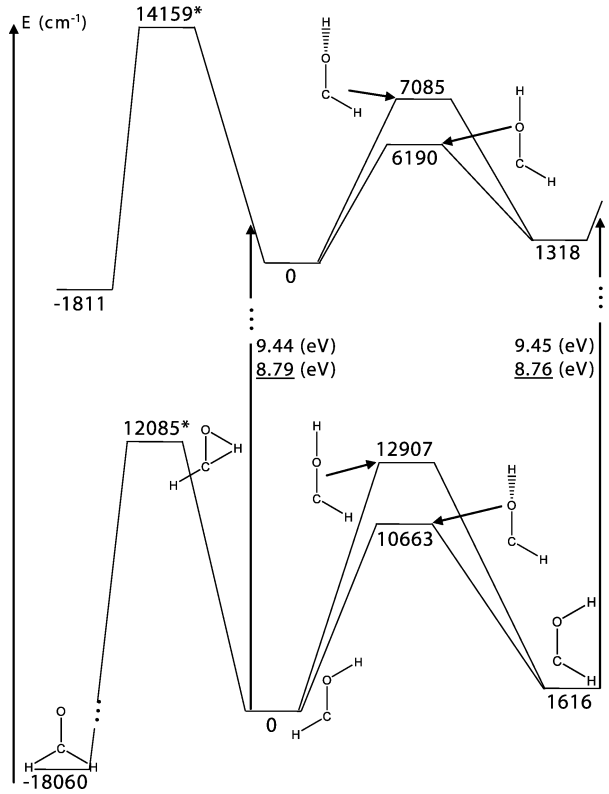


**Figure 1.** Stationary points on the HCOH (lower, CCSD(T)/cc-pVTZ) and $HCOH^+$ (upper) PES. Vertical arrows represent ionization to the Franck−Condon regions and vertical (regular print) and adiabatic (underline) IEs are given. Energies of stationary points are listed on each surface relative to their global minimum (trans structure). The formaldehyde isomer was not included in our PES, and the associated barrier (marked with an asterisk (*)) was calculated with CCSD(T)/cc-pVTZ at the B3LYP/cc-pVTZ optimized transition state.

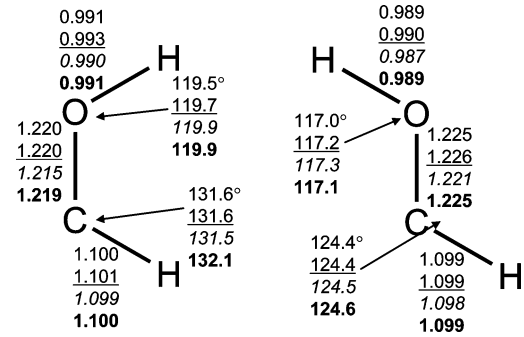


**Figure 2.** Equilibrium structures on the cation PES. CCSD(T)/cc-pVTZ (regular print), CCSD(T)/aug-cc-pVTZ (underline), CCSD(T)/cc-pVQZ (italic), and PES (bold) for *cis*- (left) and *trans*-$HCOH^+$ (right). $E_{nuc}$ = 31.858 717 au and 31.825 806 au at the CCSD(T)/cc-pVTZ (frozen core) geometries. All calculations were performed with core electrons frozen.



the ionized system. The information about changes in electronic wave functions can be inferred from the vibrational progressions due to structural changes by using Koopmans-like arguments. Although the Koopmans theorem[24] neglects electron correlation and orbital relaxation effects, it provides useful qualitative guidelines for rationalizing and predicting structural changes upon ionization. Moreover, a simple one-electron picture of the ionization process can be developed for correlated wave functions by using Dyson orbitals.[25]

Vibrational progressions give frequencies and anharmonicities on the upper state and information about structural differences between the two states. This is the focus of this paper, which is organized as follows. Section II discusses theory and computational details, including basis set convergence, details of the vibrational configuration interaction (VCI) basis, and calculation of the Franck−Condon factors. Section III discusses the molecular orbitals and structural changes upon ionization, as well as barriers on the potential energy surface (PES). Section IV discusses the vibrational levels of $HCOH^+$ and presents the photoelectron spectra, and Section V does the same for the deuterated isomers HCOD. Section VI compares the VCI photoelectron spectra with the harmonic parallel-mode approximation and shows that better accuracy is obtained by calculating displacements along the cation normal coordinates. Finally, Section VII presents our conclusions.

## II. Theory and Computational Details

The calculations employed PESs for the neutral and cation ground states. The neutral PES is described in our early publication.[9] The new cation surface covers the cis and trans wells and the space connecting them. Both PESs are available for download along with precompiled ezPES software.[26]

The PES is a 9th degree polynomial in Morse variables of the set of interatomic distances, represented in a specially constructed basis invariant to permutations of like nuclei. The Morse variables are defined as: $y(i, j) = e^{-r(i,j)/\lambda}$. $r(i, j)$ is the internuclear distance between atoms $i$ and $j$, and on the basis of previous optimization studies, the value of $\lambda$ is set to 2 bohr. Any value in the range 1.5 to 2.5 bohr will yield similar fitting precision, on the basis of our extensive experience using Morse variables in fitting PESs. The polynomial contains 2649 terms fitted by weighted data to 26,221 ab initio single point energies, calculated by the CCSD(T) method[27,28] with the cc-pVTZ basis set.[29] The restricted open-shell Hartree−Fock was used as a reference to mitigate the effects of spin contamination. The PES was fitted to 22 263 points in the range [0, 0.1) a.u. above the global minimum (*trans*-$HCOH^+$ equilibrium structure), 1903 points in the range [0.1, 0.2) a.u., and 1894 points in the range [0.2, 0.5) a.u. The least squares was weighted to ensure low-energy points were well-fitted and harmonic frequencies reproduced ab initio values. The rms fitting errors are 24 $cm^{-1}$ below 3000 $cm^{-1}$, 44 $cm^{-1}$ below 5000 $cm^{-1}$, and 62 $cm^{-1}$ below the highest barrier at 7085 $cm^{-1}$. Points above 0.1 au were included to enforce asymptotes for fragmentation and small internuclear distances. The calculations were performed using MOLPRO.[30] The core electrons were frozen in all PES calculations. Similarly constructed PESs have been used in several dynamics, and spectroscopy studies[31−37] details of constructing the symmetrized polynomial basis are given elsewhere.[38]

Basis set effects were considered by examining equilibrium structures and frequencies with the aug-cc-pVTZ[39] and cc-pVQZ bases[29] (Figure 2). Bond lengths and angles are well-converged at the cc-pVTZ level. The largest differences are a 0.005 Å decrease in the CO bond length and a 0.4° increase in the H−O−C angle. Harmonic frequencies are also well-converged. Average absolute differences are 7.9 $cm^{-1}$ between cc-pVTZ and aug-cc-pVTZ and 5.0 $cm^{-1}$ between cc-pVTZ and cc-pVQZ. Basis set convergence is better with respect to polarization than diffuse functions, implying some diffuse character of the electron density. The OH stretch is most sensitive to this: its frequency decreases by 16 $cm^{-1}$ upon adding diffuse functions, but remains unchanged with added polarization.

The PES replicates equilibrium CCSD(T)/cc-pVTZ bond lengths to 0.001 Å, and bond angles to 0.2° in *trans*- and 0.5° in *cis*-$HCOH^+$ (Figure 2). Frequencies on the PES were

**TABLE 1: Comparison of Harmonic Frequencies ($cm^{-1}$) and IR Intensities (km/mol, in parentheses) for *cis*-$HCOH^+$**

| | mode | symmetry | cc-pVTZ[a] | cc-pVTZ[b] | PES[c] | aug-cc-pVTZ[b] | cc-pVQZ[b] |
|---|---|---|---|---|---|---|---|
| $\nu_6$ | op. wag | a″ | 935 (32) | 931 | 931 | 921 | 924 |
| $\nu_5$ | ip bend | a′ | 988 (65) | 987 | 996 | 984 | 984 |
| $\nu_4$ | ip bend | a′ | 1171 (176) | 1173 | 1159 | 1166 | 1169 |
| $\nu_3$ | CO stretch | a′ | 1733 (73) | 1716 | 1711 | 1710 | 1724 |
| $\nu_2$ | CH stretch | a′ | 3085 (45) | 3055 | 3054 | 3047 | 3054 |
| $\nu_1$ | OH stretch | a′ | 3464 (339) | 3448 | 3442 | 3428 | 3446 |

[a] ACES II using analytic gradients; all electrons are correlated. [b] MOLPRO using finite differences; core electrons are frozen. [c] Finite-differences calculations using PES fitted to the cc-pVTZ (frozen core) results.

**TABLE 2: Comparison of Harmonic Frequencies ($cm^{-1}$) and IR Intensities (km/mol, in parentheses) for *trans*-$HCOH^+$**

| | mode | symmetry | cc-pVTZ[a] | cc-pVTZ[b] | PES[c] | aug-cc-pVTZ[b] | cc-pVQZ[b] |
|---|---|---|---|---|---|---|---|
| $\nu_6$ | op wag | a″ | 966 (157) | 965 | 970 | 965 | 958 |
| $\nu_5$ | ip bend | a′ | 998 (213) | 999 | 997 | 994 | 987 |
| $\nu_4$ | ip bend | a′ | 1257 (33) | 1255 | 1254 | 1249 | 1246 |
| $\nu_3$ | CO stretch | a′ | 1706 (87) | 1692 | 1694 | 1685 | 1699 |
| $\nu_2$ | CH stretch | a′ | 3097 (58) | 3073 | 3069 | 3066 | 3073 |
| $\nu_1$ | OH stretch | a′ | 3529 (413) | 3511 | 3499 | 3495 | 3511 |

[a] ACES II using analytic gradients, all electrons are correlated. [b] MOLPRO using finite differences, core electrons are frozen. [c] Finite-differences calculations using PES fitted to the cc-pVTZ (frozen core) results.



calculated numerically using 5-point central difference formulas. They reproduce CCSD(T) finite difference frequencies with an average (absolute) difference of 5.8 and 4.3 $cm^{-1}$ for *cis*- and *trans*-$HCOH^+$, respectively, and maximum differences of 14 and 12 $cm^{-1}$ (Tables 1, 2). To emphasize the character of the motion, we refer to some bending motions as "in-plane" and "out-of-plane" bends, instead of the conventional "bend" and "wag" terms used to describe planar and nonplanar motions, respectively.

Vibrational energies and wave functions were calculated by diagonalizing the Watson Hamiltonian[40] for $J = 0$ (pure vibration) in a basis of vibrational self-consistent field[41] (VSCF) functions. The basis for VSCF optimized modals was the set of harmonic oscillator wave functions along the normal coordinates, with quantum numbers from 0 to 15. Multimode interactions in the PES were included up to the 4-mode level. The rovibrational corrections were treated in an approximate manner. The Watson correction term was calculated in the *n*-mode representation along with the potential, up to the 4-mode level.[42] Coriolis coupling terms that coupled two modes were integrated over a 2-mode representation of the inverse moment of inertia tensor. The basis for VCI calculations consisted of all VSCF product wave functions with maximum of 10 total quanta excited from the VSCF ground state reference, with a maximum of 5 modes simultaneously excited. Matrix elements of the Hamiltonian were calculated numerically using the Gauss−Hermite quadrature with 20 integration points for 1D and 2D integrals, 15 points for 3D integrals, and 10 points for 4D integrals.

Franck−Condon factors were calculated as full-dimensional (i.e., 6-dimensional) integrals over the normal coordinates of the cation PES. The neutral ground-state wave function at each point was obtained by aligning the molecules according to center of mass and the principal axis system, transforming between the normal coordinates, and evaluating the VCI wave function. Thus, no approximations were made in evaluating Franck−Condon factors via full-dimensional integration conducted using exact transformation between the two sets of normal coordinates. Only transitions from the ground vibrational states of the neutral are considered in photoelectron spectrum calculations because these are most likely to be of relevance to future experiments.

Nonzero Franck−Condon factors were calculated for levels up to 7000 $cm^{-1}$ above the zero-point energy. With the present VCI basis, convergence in the VCI energies was converged to 1 $cm^{-1}$ for most states below 4000 $cm^{-1}$, with the exception of four combination/overtones of $\nu_6$, which are converged to about 2 $cm^{-1}$. This mode leads toward the out-of-plane transition state connecting cis and trans; large VCI bases lead to inefficient convergence, probably because they sample this flat region. Above 4000 $cm^{-1}$, convergence in these states is about 5−10 $cm^{-1}$. $\nu_6$ is the only out-of-plane mode and is not active in the photoelectron spectrum. The active states are converged to about 5 $cm^{-1}$ up to 7000 $cm^{-1}$.

Single-point energies for the PES fitting were calculated using MOLPRO.[30] Harmonic frequencies were calculated using MOLPRO and ACES II[43] and harmonic infrared intensities using ACES II. The core orbitals were frozen in all MOLPRO calculations and correlated in ACES II and Q-Chem[44] calculations. ACES II was used only to calculate harmonic frequencies using analytic gradients for comparison versus MOLPRO, which employs a finite differences procedure. MOLPRO harmonic vibrational frequencies were computed by finite differences using total energies, whereas ACES II calculations employed first analytic derivatives.[45]

All vibrational wave functions and energy levels were computed using the ezVibe code.[46] For benchmark purposes, we compared VCI levels from ezVibe with the MULTIMODE program.[47] Agreement in the energies was within 1 $cm^{-1}$ for states below 6000 $cm^{-1}$ (approximately 160 states) and within 2 $cm^{-1}$ below about 7300 $cm^{-1}$ (300 states).

## III. Molecular Orbital Framework and Structural Effects of Ionization

The smallest carbene, methylene ($CH_2$), has a triplet ground state, with two unpaired electrons on the divalent carbon atom. The singlet−triplet gap is 0.39 eV.[48,49] Substituted carbenes have diverse properties; for example, in the stereospecifity of their reactions.[17,50−52] The differences in reactivity can often be explained in terms of the singlet-versus-triplet character of the ground state.

The triplet state in carbenes has two electrons in nonbonding orbitals on carbon, one $\sigma$ and one $\pi$. The singlet state has the electrons paired in the $\sigma$ orbital, with the $\pi$ orbital unoccupied. The effect of substituents can be explained using simple molecular orbital considerations:[53,54] substituent groups with $\pi$

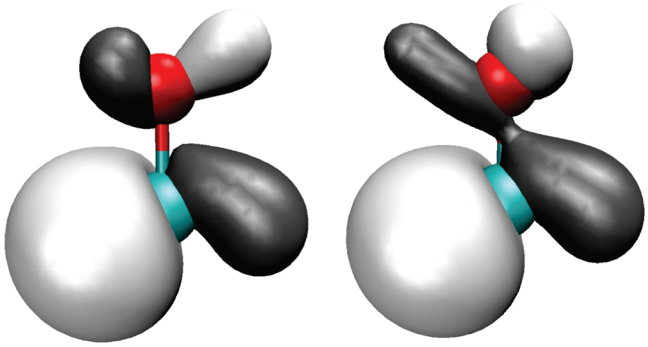

**Figure 3.** The highest occupied molecular orbital of *cis*- (left) and *trans*-HCOH (right).

**TABLE 3: Comparison of Harmonic Frequencies ($cm^{-1}$) between the Neutral and the Cation PESs**

| | op wag | ip bend | ip bend | CO stretch | CH stretch | OH stretch |
|---|---|---|---|---|---|---|
| *cis*-HCOH | 1014 | 1238 | 1476 | 1335 | 2768 | 3655 |
| *cis*-$HCOH^+$ | 931 | 996 | 1159 | 1711 | 3054 | 3442 |
| *trans*-HCOH | 1098 | 1214 | 1508 | 1326 | 2853 | 3754 |
| *trans*-$HCOH^+$ | 970 | 997 | 1254 | 1694 | 3069 | 3499 |

type lone pairs (N, O atoms) lead to singlet ground states because these lone pairs can mix with carbon's $\pi$ orbital. This can raise it enough so that pairing the electrons in $\sigma$ becomes energetically favorable. For example, in HCOH, the singlet state is about 1 eV below the triplet.

The vertical (adiabatic) IEs of HCOH are 9.45 (8.76) and 9.44 (8.79) eV for the cis and trans isomers, respectively, as computed at the CCSD(T)/cc-pVTZ level (ZPE excluded). The highest occupied molecular orbital (HOMO) on HCOH is a lone pair on carbon with a minor contribution on OH, which provides antibonding character along the CO bond. (Figure 3). The first ionization removes an electron from the HOMO, with large geometrical changes in the equilibrium structure. The CO bond is shortened by 0.097 and 0.093 Å in the cis and trans isomers, respectively. Ionization from an $sp^2$ orbital on carbon increases the carbon's overall s character; the HCO angle increases by 25.5 and 22.6°. The HOC angle also increases, by 6.1 and 9.9°.

The displaced equilibrium structures strongly affect the shape of the PES, and harmonic frequencies show strong differences upon ionization (Table 3). The largest change is in the CO stretch, which increases by 370 $cm^{-1}$ in both isomers upon ionization. This is due to the shortening of the CO bond. The CH stretching frequency increases upon ionization, by 286 and 216 $cm^{-1}$. The remaining four frequencies decrease. The OH stretch decreases by 213 and 255 $cm^{-1}$; this follows from the longer OH bond in the cation, due to increased donation into the electron-depleted carbon. The remaining three are bending modes involving the OH group; the oxygen lone pairs encounter less steric hindrance with a single electron on C in these motions.

Two barriers on the $HCOH^+$ PES, which separate the cis and trans wells, are 6190 and 7085 $cm^{-1}$ above the trans minimum (Figure 1). The respective transition states represent in-plane and out-of-plane rotation of H around the oxygen, respectively. These transition states are lower in energy relative to the neutral (by 6717 $cm^{-1}$ for the linear, and by 3578 $cm^{-1}$ for the out-of-plane). This also is due to decreased repulsion between the electrons on O and C: in out-of-plane rotation, the HOC angle remains essentially constant. In in-plane rotation, this angle changes, and the oxygen's electron density is brought closer to the carbon center. The ionized carbon atom presents a much smaller barrier for this interaction; hence, the disproportionate effect of ionization on the two barriers.

**TABLE 4: The $HCOH^+$ VCI Vibrational Levels below 3600 $cm^{-1}$, and Corresponding Levels for $HCOD^+$ ($cm^{-1}$)**

| no. | state label | *cis*-$HCOH^+$ | *cis*-$HCOD^+$ | *trans*-$HCOH^+$ | *trans*-$HCOD^+$ |
|---|---|---|---|---|---|
| 1 | $\nu_6$ | 905 | 746 | 935 | 781 |
| 2 | $\nu_5$ | 949 | 822 | 967 | 822 |
| 3 | $\nu_4$ | 1126 | 1099 | 1211 | 1143 |
| 4 | $\nu_3$ | 1684 | 1671 | 1664 | 1655 |
| 5 | $2\nu_6$ | 1811 | 1475 | 1858 | 1547 |
| 6 | $\nu_5+\nu_6$ | 1874 | 1575 | 1915 | 1604 |
| 7 | $2\nu_5$ | 1885 | 1641 | 1933 | 1644 |
| 8 | $\nu_4+\nu_6$ | 2045 | 1835 | 2149 | 1912 |
| 9 | $\nu_4+\nu_5$ | 2052 | 1947 | 2141 | 1982 |
| 10 | $2\nu_4$ | 2224 | 2167 | 2405 | 2259 |
| 11 | $\nu_3+\nu_6$ | 2582 | 2436 | 2597 | 2417 |
| 12 | $\nu_3+\nu_5$ | 2624 | 2488 | 2626 | 2477 |
| 13 | $3\nu_6$ | 2711 | 2193 | 2779 | 2301 |
| 14 | $\nu_5+2\nu_6$ | 2782 | 2306 | 2826 | 2365 |
| 15 | $\nu_3+\nu_4$ | 2801 | 2753 | 2863 | 2785 |
| 16 | $3\nu_5$ | 2823 | 2456 | 2908 | 2463 |
| 17 | $2\nu_5+\nu_6$ | 2825 | 2395 | 2903 | 2430 |
| 18 | $\nu_2$ | 2896 | 2384 | 2933 | 2478 |
| 19 | $\nu_4+2\nu_5$ | 2954 | 2784 | 3054 | 2818 |
| 20 | $\nu_4+2\nu_6$ | 2962 | 2557 | 3100 | 2671 |
| 21 | $\nu_4+\nu_5+\nu_6$ | 2990 | 2691 | 3090 | 2751 |
| 22 | $2\nu_4+\nu_5$ | 3122 | 3038 | 3298 | 3109 |
| 23 | $2\nu_4+\nu_6$ | 3156 | 2877 | 3340 | 3016 |
| 24 | $\nu_1$ | 3248 | 2900 | 3328 | 2927 |
| 25 | $3\nu_4$ | 3300 | 3191 | 3578 | 3347 |
| 26 | $2\nu_3$ | 3347 | 3321 | 3306 | 3287 |
| 27 | $\nu_3+2\nu_6$ | 3481 | 3176 | 3519 | 3177 |
| 28 | $\nu_3+\nu_5+\nu_6$ | 3542 | 3253 | 3574 | 3285 |
| 29 | $\nu_3+2\nu_5$ | 3560 | 3304 | 3589 | 3301 |

It should be noted that Figure 1 in our previous paper[9] had a typographical error: energies of the two barriers connecting *cis*- and *trans*-HCOH were incorrectly labeled relative to the cis minimum, rather than to the trans, as indicated. In addition, the neutral PES was optimized to replicate harmonic frequencies; we have since created a similar PES that replicates barrier heights accurately with only a moderate decline in the accuracy of the harmonic frequencies. Both PESs are available for download from the iOpenShell Web site.

## IV. Photoelectron Spectra of HCOH

Vibrational levels of $HCOH^+$ up to 3600 $cm^{-1}$ are listed in Table 4. Considering the fundamental excitations, the first four levels (up to 1700 $cm^{-1}$) are accurately described by the harmonic approximation, with an average deviation between harmonic and VCI excitation energies of 35 $cm^{-1}$. The higher stretches show large deviations from the harmonic approximation; VCI decreases the CH and OH stretch fundamental frequencies by approximately 150 and 190 $cm^{-1}$, respectively.

The photoelectron spectra for the two isomers are shown in Figure 5, and positions and intensities are tabulated in Tables 5 and 6. The intensities are unitless; an intensity of 1 corresponds to full overlap between the neutral and cation wave functions.

The *cis*-HCOH photoelectron spectrum is given in Figure 5 and Table 5. In the low-energy region (0−2000 $cm^{-1}$), the lowest-frequency mode, $\nu_6$, has no intensity. This is the only mode that is not fully symmetric. If this normal mode was separable in the PES, then transitions to odd levels would be forbidden by symmetry. The other four fundamentals in this range have appreciable intensity, with $\nu_5$ and $2\nu_5$ being the strongest. In *cis*-$HCOH^+$, $\nu_5$ is a scissoring of OH and CH, which moves the molecule toward linearity. From Figure 4, displacement along this mode brings the cation into the Franck−Condon region. $\nu_4$ increases one angle and decreases the other one. It is active because the difference in H−C−O angles in neutral and cation structures is much larger than the

**TABLE 5: Active Vibrational Levels of *cis*-HCOH$^+$ /HCOD$^+$ in the Photoelectron Spectrum of *cis*-HCOH/HCOD[a]**

| | *cis*-HCOH$^+$ | | | *cis*-HCOD$^+$ | | |
|---|---|---|---|---|---|---|
| no. | state label | energy | intensity | state label | energy | intensity |
| 0 | 0 | 0 | 0.0104 | 0 | 0 | 0.0098 |
| 1 | $\nu_5$ | 949 | 0.0202 | $\nu_5$ | 746 | 0.0091 |
| 2 | $\nu_4$ | 1126 | 0.0121 | $\nu_4$ | 1099 | 0.0222 |
| 3 | $\nu_3$ | 1684 | 0.0144 | $\nu_3$ | 1671 | 0.0148 |
| 4 | $2\nu_5$ | 1885 | 0.0163 | $\nu_4+\nu_5$ | 1835 | 0.0222 |
| 5 | $\nu_4+\nu_5$ | 2052 | 0.0312 | $2\nu_4$ | 2167 | 0.0279 |
| 6 | $2\nu_4$ | 2224 | 0.0075 | $\nu_2$ | 2384 | 0.0068 |
| 7 | $\nu_3+\nu_5$ | 2624 | 0.0265 | $\nu_4+2\nu_5$ | 2557 | 0.0076 |
| 8 | $\nu_3+\nu_4$ | 2801 | 0.0062 | $\nu_3+\nu_4$ | 2753 | 0.0267 |
| 9 | $3\nu_5$ | 2823 | 0.0140 | $2\nu_4+\nu_5$ | 2877 | 0.0342 |
| 10 | $\nu_4+2\nu_5$ | 2954 | 0.0218 | $3\nu_4$ | 3191 | 0.0226 |
| 11 | $\nu_4+2\nu_6$ | 2962 | 0.0186 | $2\nu_3$ | 3321 | 0.0107 |
| 12 | $2\nu_4+\nu_5$ | 3122 | 0.0173 | $\nu_2+\nu_4$ | 3461 | 0.0156 |
| 13 | $2\nu_3$ | 3347 | 0.0102 | $\nu_2+\nu_4$ | 3511 | 0.0084 |
| 14 | $\nu_3+2\nu_5$ | 3560 | 0.0208 | $2\nu_4+2\nu_5$ | 3589 | 0.0151 |
| 15 | $\nu_3+\nu_4+\nu_5$ | 3714 | 0.0185 | $\nu_3+2\nu_4$ | 3809 | 0.0205 |
| 16 | $4\nu_5$ | 3776 | 0.0184 | $3\nu_4+\nu_5$ | 3859 | 0.0298 |
| 17 | $\nu_4+3\nu_5$ | 3865 | 0.0295 | $\nu_2+\nu_4+\nu_5$ | 4180 | 0.0101 |
| 18 | $\nu_3+2\nu_4$ | 3891 | 0.0176 | $2\nu_3+\nu_4$ | 4389 | 0.0149 |
| 19 | $2\nu_4+2\nu_5$ | 4008 | 0.0069 | $\nu_3+2\nu_4+\nu_5$ | 4501 | 0.0236 |
| 20 | $\nu_2+\nu_4$ | 4022 | 0.0100 | $3\nu_4+2\nu_5$ | 4565 | 0.0233 |
| 21 | $2\nu_3+\nu_5$ | 4279 | 0.0165 | $\nu_3+3\nu_4$ | 4844 | 0.0386 |
| 22 | $\nu_3+3\nu_5$ | 4502 | 0.0171 | $2\nu_3+\nu_4+\nu_5$ | 5096 | 0.0112 |
| 23 | $\nu_3+\nu_4+2\nu_5$ | 4619 | 0.0244 | $\nu_3+2\nu_4+2\nu_5$ | 5217 | 0.0131 |
| 24 | $5\nu_5$ | 4730 | 0.0196 | $2\nu_3+2\nu_4$ | 5438 | 0.0099 |
| 25 | $\nu_2+\nu_5+\nu_6$ | 4740 | 0.0083 | $\nu_3+3\nu_4+\nu_5$ | 5482 | 0.0160 |
| 26 | $\nu_4+5\nu_5$ | 4814 | 0.0319 | $2\nu_3+3\nu_5$ | 5486 | 0.0122 |
| 27 | $2\nu_3+2\nu_5$ | 5215 | 0.0116 | $4\nu_4+2\nu_5$ | 5549 | 0.0187 |
| 28 | $\nu_3+4\nu_5$ | 5464 | 0.0238 | $\nu_3+4\nu_4$ | 5839 | 0.0174 |
| 29 | $\nu_3+\nu_4+3\nu_5$ | 5553 | 0.0351 | $2\nu_3+2\nu_4+\nu_5$ | 6139 | 0.0120 |
| 30 | $\nu_3+2\nu_4+2\nu_5$ | 5723 | 0.0240 | $\nu_3+3\nu_4+2\nu_5$ | 6236 | 0.0112 |
| 31 | $2\nu_3+3\nu_5$ | 6166 | 0.0074 | | | |
| 32 | $\nu_2+\nu_3+2\nu_5$ | 6389 | 0.0083 | | | |
| 33 | $\nu_3+5\nu_5$ | 6466 | 0.0209 | | | |
| 34 | $\nu_3+\nu_4+4\nu_5$ | 6529 | 0.0177 | | | |

[a] Energies are in cm$^{-1}$ and intensities are unitless.

**TABLE 6: Active Vibrational Levels of *trans*-HCOH$^+$ /HCOD$^+$ in the Photoelectron Spectrum of *trans*-HCOH/HCOD[a]**

| | *trans*-HCOH$^+$ | | | *trans*-HCOD$^+$ | | |
|---|---|---|---|---|---|---|
| no. | state label | energy | intensity | state label | energy | intensity |
| 0 | 0 | 0 | 0.0155 | 0 | 0 | 0.0144 |
| 1 | $\nu_5$ | 967 | 0.0062 | $\nu_4$ | 1143 | 0.0419 |
| 2 | $\nu_4$ | 1211 | 0.0390 | $\nu_3$ | 1655 | 0.0193 |
| 3 | $\nu_3$ | 1664 | 0.0200 | $2\nu_4$ | 2259 | 0.0644 |
| 4 | $\nu_4+\nu_5$ | 2141 | 0.0162 | $\nu_3+\nu_4$ | 2785 | 0.0483 |
| 5 | $2\nu_4$ | 2405 | 0.0515 | $2\nu_3$ | 3287 | 0.0090 |
| 6 | $\nu_3+\nu_5$ | 2626 | 0.0071 | $3\nu_4$ | 3347 | 0.0703 |
| 7 | $\nu_3+\nu_4$ | 2863 | 0.0371 | $\nu_3+2\nu_4$ | 3894 | 0.0676 |
| 8 | $\nu_2$ | 2933 | 0.0102 | $2\nu_3+\nu_4$ | 4411 | 0.0786 |
| 9 | $2\nu_4+\nu_5$ | 3298 | 0.0124 | $\nu_2+2\nu_4$ | 4714 | 0.0075 |
| 10 | $2\nu_3$ | 3306 | 0.0218 | $\nu_3+3\nu_4$ | 4979 | 0.0642 |
| 11 | $3\nu_4$ | 3578 | 0.0450 | $5\nu_4$ | 5459 | 0.0336 |
| 12 | $\nu_3+\nu_4+\nu_5$ | 3794 | 0.0150 | $2\nu_3+2\nu_4$ | 5512 | 0.0361 |
| 13 | $\nu_3+2\nu_4$ | 4049 | 0.0427 | $\nu_2+3\nu_4$ | 5791 | 0.0084 |
| 14 | $\nu_2+\nu_4$ | 4144 | 0.0118 | $\nu_2+\nu_3+\nu_4+\nu_5$ | 6046 | 0.0220 |
| 15 | $2\nu_4+2\nu_5$ | 4207 | 0.0126 | $\nu_3+4\nu_4$ | 6047 | 0.0357 |
| 16 | $3\nu_4+\nu_5$ | 4449 | 0.0179 | $6\nu_4$ | 6520 | 0.0174 |
| 17 | $2\nu_3+\nu_4$ | 4498 | 0.0225 | | | |
| 18 | $4\nu_4$ | 4736 | 0.0312 | | | |
| 19 | $\nu_3+2\nu_4+\nu_5$ | 4950 | 0.0216 | | | |
| 20 | $\nu_3+3\nu_4$ | 5221 | 0.0277 | | | |
| 21 | $3\nu_4+2\nu_5$ | 5372 | 0.0131 | | | |
| 22 | $4\nu_4+\nu_5$ | 5606 | 0.0109 | | | |
| 23 | $2\nu_3+2\nu_4$ | 5674 | 0.0195 | | | |
| 24 | $5\nu_4$ | 5883 | 0.0091 | | | |
| 25 | $3\nu_3+\nu_4$ | 6114 | 0.0166 | | | |
| 26 | $\nu_3+4\nu_4$ | 6378 | 0.0218 | | | |
| 27 | $2\nu_3+2\nu_4+\nu_5$ | 6587 | 0.0113 | | | |
| 28 | $2\nu_3+3\nu_4$ | 6845 | 0.0161 | | | |

[a] Energies are in cm$^{-1}$ and intensities are unitless.

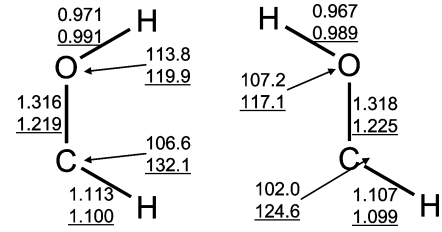


**Figure 4.** Equilibrium structures calculated on the PES for HCOH (regular print) and HCOH$^+$ (underline) for cis (left) and trans (right) isomers. All calculations were performed with core electrons frozen.

difference in H−O−C angles. The third active mode is $\nu_3$, which is the CO stretch.

In the high energy range (2000−7000 cm$^{-1}$), six peaks have significant intensity (greater than ∼0.025). Peaks labeled 5, 7, and 17 are composed of primarily one VSCF state and correspond to combination bands of two modes, $\nu_5$ and either $\nu_4$ (5 and 17, more intense) or $\nu_3$ (7, less intense). Peaks 23, 26, and 29 are combinations in all three active modes and mix several (2−8) VSCF states. All of the intense peaks in the *cis*-HCOH spectrum represent vibrational states with multiple quanta in combinations of $\nu_5$ and $\nu_4$ and, to a smaller extent, $\nu_3$.

The *trans*-HCOH spectrum is given in Figure 5 and Table 6. It is qualitatively different from that for *cis*-HCOH: there are fewer intense progressions, and they occur at much lower energies. $\nu_4$ at 1211 cm$^{-1}$ dominates the low-energy part of the spectrum, with $\nu_3$ having about half the intensity. $\nu_4$ is the bend that brings the molecule to linearity, and $\nu_3$ is the CO stretch. Above 2000 cm$^{-1}$, the five strongest peaks occur below 4050 cm$^{-1}$. The dominant progression throughout the spectrum is an overtone of $\nu_4$. Other peaks with lesser intensity are combination bands involving excited quanta in $\nu_3$ and $\nu_4$. Compared to the cis isomer, *trans*-HCOH shows a less dense spectrum, with most of the intensity in $\nu_4$.

The qualitative differences in the two photoelectron spectra can be rationalized by differences in equilibrium structures upon ionization (Figure 4). As discussed in Section III, the opening up of the H−C−O angle is the most prominent effect, followed by a smaller opening of the H−O−C angle. The third difference is a shortening of the CO bond in both isomers. The intensity in the photoelectron spectra of HCOH is dominated by combination bands of the two hydrogen bending modes, whose primary displacement is changing these angles. A smaller amount of intensity is seen in the CO stretch. Thus, to a great extent, the progressions in the photoelectron spectrum are due to the Condon reflection principle.[55]

## V. Photoelectron Spectra of HCOD

The photoelectron spectra for *cis*- and *trans*-HCOD are depicted in Figure 6 and tabulated in Tables 5 and 6. Compared to HCOH, the energies of all the states are decreased due to the larger mass of D; the relative intensities also change because the different mass affects the normal modes. The normal modes tend to localize vibration into H and suppress it in D. This effect is largest in *trans*-HCOD.

## VI. Comparison with the Parallel-Mode Harmonic Approximation

Franck−Condon factors between two electronic states are often approximated by assuming that (a) the vibrational wave

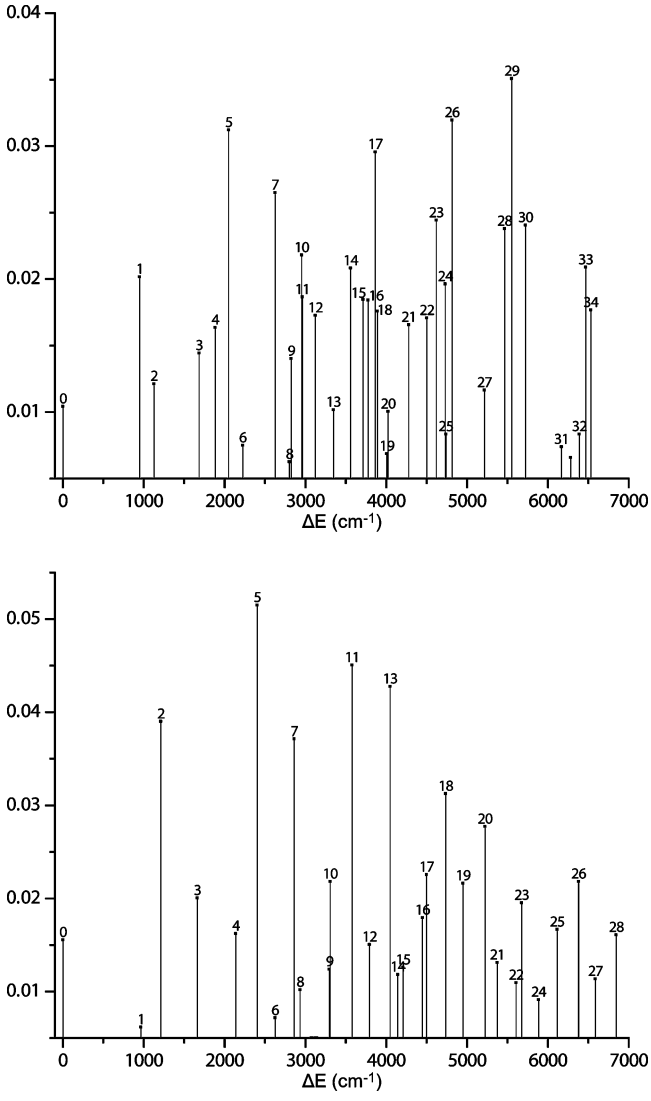


**Figure 5.** Franck−Condon factors for HCOH ionization producing the electronic ground state of $HCOH^+$ in the range from the ZPE (0 $cm^{-1}$) to 7000 $cm^{-1}$. Top, cis isomer; bottom, trans isomer.

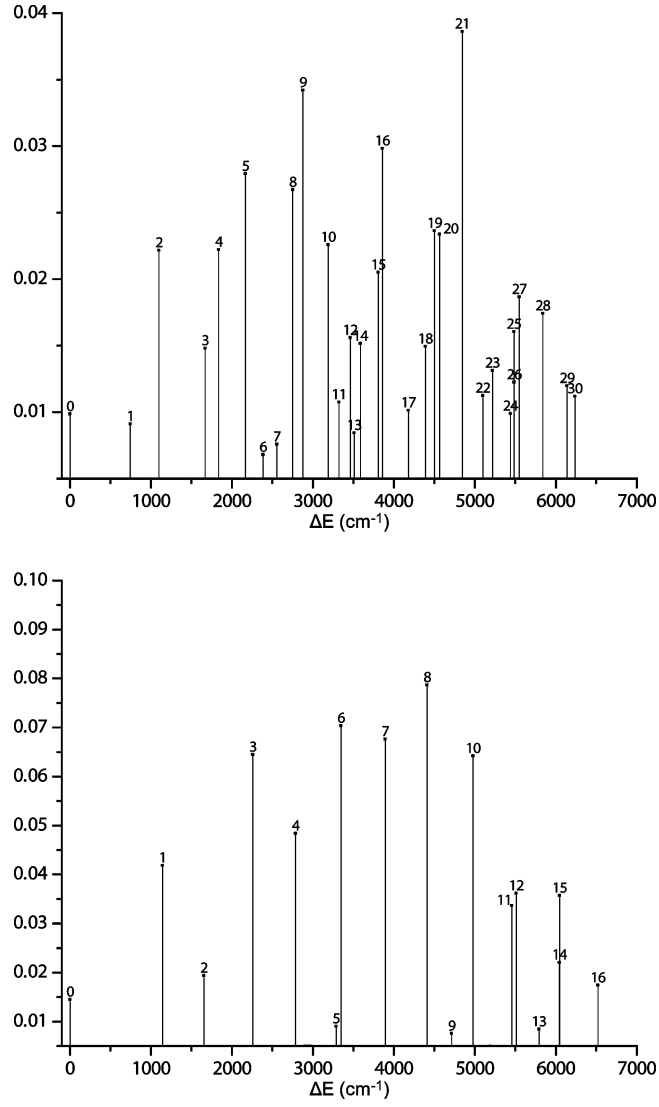


**Figure 6.** Franck−Condon factors for HCOD ionization producing the electronic ground state of $HCOD^+$ in the range from the ZPE (0 $cm^{-1}$) to 7000 $cm^{-1}$. Top, cis isomer; bottom, trans isomer.

functions are harmonic and (b) all normal coordinates on the two surfaces are parallel; that is, completely neglecting the Duschinsky rotations.[56] In this case, the Franck−Condon factors are products of 1D integrals over harmonic oscillator wave functions, which are shifted by displacement $\Delta Q$ between the equilibrium structures along that normal coordinate. Because of the neglect of rotations, $\Delta Q$ depends on the choice of normal modes used for calculation. The spectra of HCOH calculated using the two sets of normal coordinates are compared to the VCI spectrum for both isomers. All spectra were generated using CCSD(T)/cc-pVTZ frequency calculations and the ezSpectrum program.[57]

Figure 7 compares parallel-mode spectra with the VCI spectrum for the cis isomer. The parallel-mode spectra are calculated using normal coordinates of the neutral (top column in Figure 7) and the cation (bottom column) normal coordinates. The displacements differ significantly only along one coordinate, the CO stretch; $\Delta Q$ equals 0.08 and 0.21 Å $(amu)^{1/2}$ for neutral and cation normal coordinates, respectively. The differences are due to rotations (mixing); the CO bond is longer in the neutral; other modes, especially the stretches, have relative displacements along CO in their motion. Since the bends have to be displaced significantly to account for the change in H−O−C and H−C−O angles (by 0.35 and 0.33 Å $(amu)^{1/2}$ in the neutral and the cation, respectively), $\Delta Q$ along the CO stretch is smaller in the neutral coordinates. Consequently the photoelectron spectrum using the neutral normal coordinates shows negligible intensity in the CO stretch fundamental (peak 3 in Figure 7) and underestimates the intensity of all states with quanta in this mode.

Figure 8 compares this approximation with VCI for *trans*-HCOH. The same effect is seen, except that the $\Delta Q$'s differ in one of the bending modes rather than the CO stretch (peak 1 in Figure 8). The displacements are 0.05 and 0.15 Å $(amu)^{1/2}$ in the neutral and cation normal coordinates, respectively.

The effect of normal coordinate rotation on the wave function overlap between states is shown in Figure 9. On the lower state, only the ground vibrational wave function is considered (in the absence of hot bands). The errors in FCFs due to rotation of the ground vibrational wave function depend on two factors: the displacement $\Delta Q$ and the difference in frequencies of the active normal modes: if these frequencies are very similar, errors are small (column b in Figure 9). In HCOH, the three active frequencies are within 238 and 294 $cm^{-1}$ of each other for cis and trans, respectively. On the upper state, all of the wave functions are considered. For excited vibrational wave functions, even small rotations can significantly affect the overlap due to

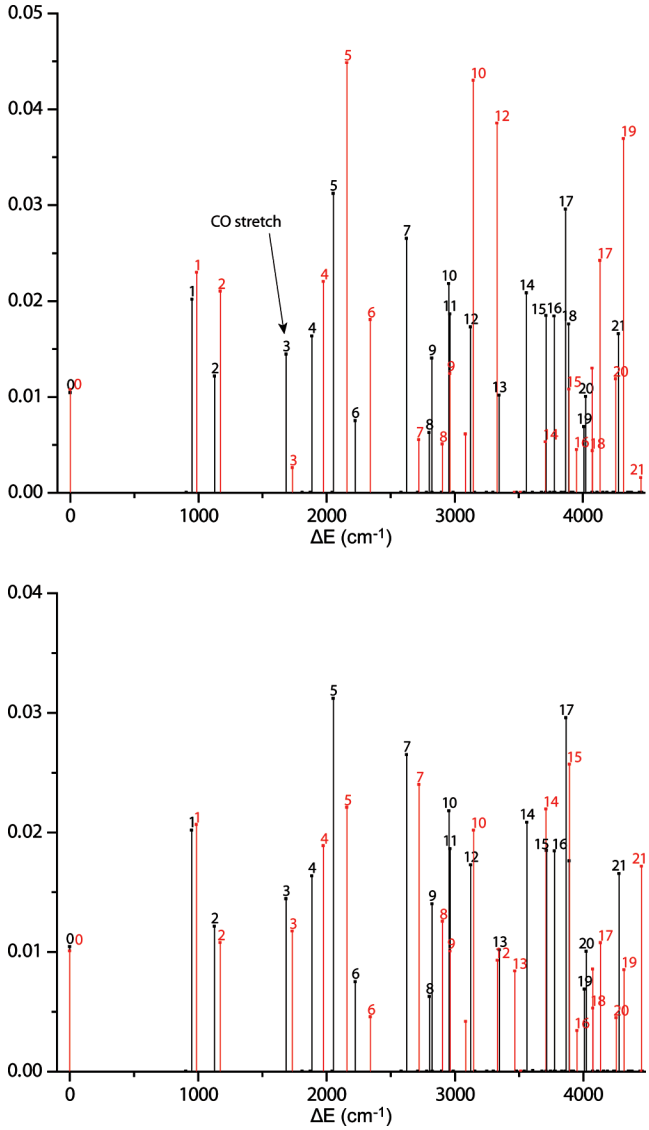


**Figure 7.** Comparison between VCI (black lines) and parallel-mode harmonic oscillator approximation (red lines) using normal coordinates of the neutral (top) and cation (bottom) for the Franck−Condon factors of *cis*-HCOH. Harmonic intensities are not scaled to match VCI.

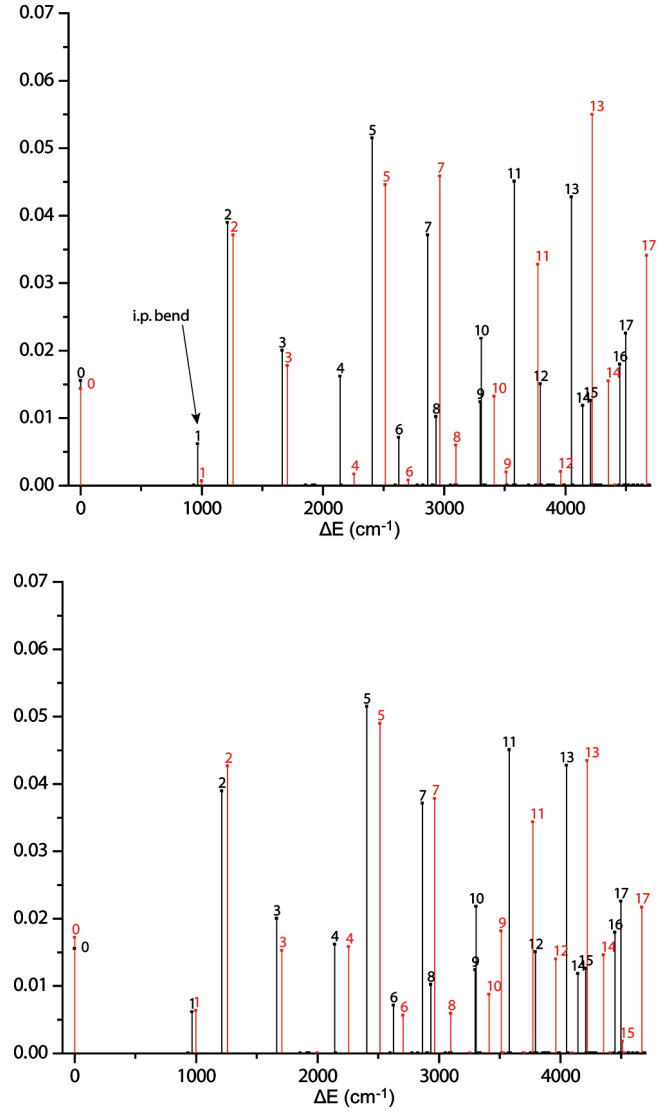


**Figure 8.** Comparison between VCI (black lines) and parallel-mode harmonic oscillator approximation (red lines) using normal coordinates of the neutral (top) and cation (bottom) for the Franck−Condon factors of *trans*-HCOH. Harmonic intensities are not scaled to match VCI.

the nodal structure (column c in Figure 9). Therefore, for large relative rotations of normal coordinates, it can be more accurate to use the normal coordinates of the cation within the parallel-mode approximation, especially if the active modes have similar frequencies on the neutral state.

## VII. Conclusions

We report accurate configuration interaction calculations of vibrational levels of the cis and trans isomers of $HCOH^+$ and $HCOD^+$. The photoelectron spectra from the ground vibrational wave functions of the two neutral isomers are also presented.

$HCOH^+$ is derived by removing an electron from a doubly occupied lone pair orbital on the carbon atom (Figure 3), with antibonding contribution along CO. This leads to large structural changes upon ionization, including shortening of the CO bond and an increase in the H−C−O angle due to increased s hybridization on C. Changes in harmonic frequency are due to structural changes and in the reduced repulsion between electrons on O and the C center in the cation.

VCI fundamental excitations are within 35 $cm^{-1}$ of the harmonic ones for the lowest four normal modes, whereas the CH and OH stretches show anharmonicities over 150 $cm^{-1}$. Due to the large difference in equilibrium structures on the neutral and cation surfaces, nonzero Franck−Condon factors are calculated for energies up to 7000 $cm^{-1}$. The progressions are localized into select frequencies; namely, two in-plane bends and the CO stretch. This is rationalized in terms of the geometrical differences. Photoelectron spectra for the HCOD isotopes are significantly different from those for HCOH; this is due to the suppression of D motion in the normal mode vibrations.

The photoelectron spectra in the parallel-mode harmonic approximation were also calculated and compared with the VCI spectra. This approximation was fairly accurate for the low-energy part of the spectrum, especially in duplicating intensities of the three active fundamental excitations in both isomers. For combinations and overtones, the harmonic intensities for the strong peaks are accurate only to within a factor of 2 for *cis*-HCOH. However, the parallel-mode harmonic approximation is slightly more accurate for *trans*-HCOH than for *cis*-.

The calculated photoelectron spectra for *cis*- and *trans*-HCOH are qualitatively different, which should make an experimental identification possible. Moreover, these differences are present

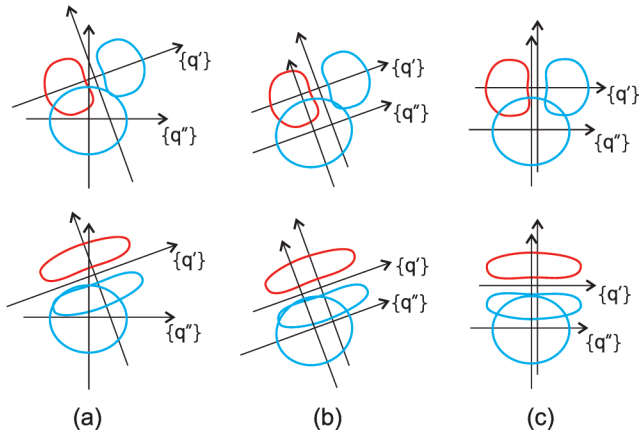


**Figure 9.** The effect of rotations of normal coordinates on Franck−Condon factors within the parallel-mode approximation. (a) The correct overlap between wave functions on lower (q″) and upper (q′) surfaces. (b) The overlap when lower normal coordinates are rotated to coincide with upper coordinates. (c) The overlap when upper normal coordinates are rotated to coincide with lower coordinates.

even in the low-energy part of the spectrum (below 2000 $cm^{-1}$), where the VCI method is expected to have the highest accuracy. Our previous work, which calculated infrared spectra of the HCOH isomers, achieved excellent agreement with experiment; we expect that current results will be of use in an experimental discrimination of the photoelectron spectra of HCOH.

**Acknowledgment.** This work is conducted under the auspices of the *iOpenShell* Center for Computational Studies of Electronic Structure and Spectroscopy of Open-Shell and Electronically Excited Species supported by the National Science Foundation through the CRIF:CRF CHE-0625419 + 0624602 + 0625237 grant. A.I.K. and J.M.B. also acknowledge support of the Department of Energy (DE-FG02-05ER15685 and DE-FG02-97ER14782, respectively).

## References and Notes

(1) Houston, P. L.; Moore, C. B. *J. Chem. Phys.* **1976**, *65*, 757.
(2) Hoffmann, M. R.; Schaeffer, H. F. *Astrophys. J.* **1981**, *249*, 563.
(3) Kemper, M. J. H.; van Dijk, J. M. F.; Buck, H. M. *J. Am. Chem. Soc.* **1978**, *100*, 7841.
(4) Hwang, D.; Mebel, A. M.; Wang, B. *Chem. Phys.* **1999**, *244*, 143.
(5) Schreiner, P. R.; Reisenauer, H. P. *ChemPhysChem* **2006**, *7*, 880.
(6) Feng, L.; Demyanenko, A. V.; Reisler, H. *J. Chem. Phys.* **2004**, *120*, 6524.
(7) Feng, L.; Demyanenko, A. V.; Reisler, H. *J. Chem. Phys.* **2003**, *118*, 9623.
(8) Schreiner, P. R.; Reisenauer, H. P.; Pickard, F.; Simmonett, A. C.; Allen, W. D.; Mátyus, E.; Császár, A. G. *Nature* **2008**, *453*, 906.
(9) Koziol, L.; Wang, Y.; Braams, B. J.; Bowman, J. M.; Krylov, A. I. *J. Chem. Phys.* **2008**, *128*, 204310.
(10) Berkowitz, J. *J. Chem. Phys.* **1978**, *69*, 3044.
(11) Burgers, P. C.; Mommers, A. A.; Holmes, J. L. *J. Am. Chem. Soc.* **1983**, *105*, 5976.
(12) Bouma, W. J.; Macleod, J. K.; Radom, L. *Int. J. Mass Spectrom. Ion Phys.* **1980**, *33*, 87.
(13) Wesdemiotis, C.; McLafferty, F. W. *Tetrahedron Lett.* **1981**, *22*, 3479.
(14) Ma, N. L.; Smith, B. J.; Collins, M. A.; Pople, J. A.; Radom, L. *J. Phys. Chem.* **1989**, *93*, 7759.
(15) Wiest, O. *J. Mol. Struct. (Theochem)* **1995**, *368*, 39.
(16) Yonehara, T.; Kato, S. *J. Chem. Phys.* **2002**, *117*, 11131.
(17) *Kinetics and Spectroscopy of Carbenes and Biradicals*; Platz, M. S., Ed.; Plenum Press: New York, 1990.
(18) Tao, C.; Mukarakate, C.; Brusse, D.; Mishchenko, Y.; Reid, S. A. *J. Mol. Spectrosc.* **2007**, *241*, 180.
(19) Tao, C.; Deselnicu, M.; Fan, H.; Mukarakate, C.; Ionescu, I.; Reid, S. A. *Phys. Chem. Chem. Phys.* **2006**, *8*, 707.
(20) Fan, H.; Ionescu, I.; Annesley, C.; Reid, S. A. *Chem. Phys. Lett.* **2003**, *378*, 548.
(21) Tao, C.; Ebben, C.; Ko, H.; Reid, S. A. *Phys. Chem. Chem. Phys.* **2008**, *10*, 6090.
(22) Goddard, J. G.; Schaefer, H. F. *J. Chem. Phys.* **1979**, *70*, 5117.
(23) Osamura, Y.; Goddard, J. G.; Schaefer, H. F. *J. Chem. Phys.* **1980**, *74*, 617.
(24) Koopmans, T. *Physica* **1933**, *1*, 104.
(25) Oana, M.; Krylov, A. I. *J. Chem. Phys.* **2007**, *127*, 234106.
(26) Kamarchik, E.; Braams, B.; Krylov, A. I.; Bowman, J. M. ezPES; http://iopenshell.usc.edu/downloads/.
(27) Raghavachari, K.; Trucks, G. W.; Pople, J. A.; Head-Gordon, M. *Chem. Phys. Lett.* **1989**, *157*, 479.
(28) Watts, J. D.; Gauss, J.; Bartlett, R. J. *J. Chem. Phys.* **1993**, *98*, 8718.
(29) Dunning, T. H. *J. Chem. Phys.* **1989**, *90*, 1007.
(30) Werner H.-J. et al. *MOLPRO 2002.6*; 2003.
(31) Brown, A.; Braams, B. J.; Christoffel, K. M.; Jin, Z.; Bowman, J. M. *J. Phys. Chem. A* **2003**, *199*, 8790.
(32) Huang, X.; Braams, B. J.; Carter, S.; Bowman, J. M. *J. Am. Chem. Soc.* **2003**, *126*, 5042.
(33) Brown, A.; McCoy, A. B.; Braams, B. J.; Jin, Z.; Bowman, J. M. *J. Chem. Phys.* **2004**, *121*, 4105.
(34) Park, S. C.; Braams, B. J.; Bowman, J. M. *J. Theor. Comput. Chem.* **2005**, *4*, 163.
(35) Huang, X.; Braams, B. J.; Bowman, J. M. *J. Chem. Phys.* **2005**, *122*, 044308.
(36) Huang, X.; Braams, B. J.; Bowman, J. M. *J. Phys. Chem. A* **2006**, *110*, 445.
(37) Xie, Z.; Braams, B. J.; Bowman, J. M. *J. Chem. Phys.* **2005**, *122*, 224307.
(38) Huang, X.; Braams, B. J.; Bowman, J. M. *J. Phys. Chem.* **2005**, *122*, 044308.
(39) Kendall, R. A., Jr.; Dunning, T. H.; Harrison, R. J. *J. Chem. Phys.* **1992**, *96*, 6796.
(40) Watson, J. K. G. *Mol. Phys.* **1968**, *15*, 479.
(41) Bowman, J. M. *Acc. Chem. Res.* **1986**, *19*, 202.
(42) Carter, S.; Culik, S. J.; Bowman, J. M. *J. Chem. Phys.* **1997**, *107*, 10458.
(43) Stanton, J. F.; Gauss, J.; Watts, J. D.; Lauderdale, W. J.; Bartlett, R. J. *ACES II*, 1993. The package also contains modified versions of the MOLECULE Gaussian integral program of J. Almlöf and P.R. Taylor, the ABACUS integral derivative program written by T. U. Helgaker, H. J. Aa. Jensen, P. Jørgensen, and P. R. Taylor and the PROPS property evaluation integral code of P. R. Taylor.
(44) Shao, Y.; Molnar, L. F.; Jung, Y.; Kussmann, J.; Ochsenfeld, C.; Brown, S.; Gilbert, A. T. B.; Slipchenko, L. V.; Levchenko, S. V.; O'Neil, D. P.; Distasio, R. A., Jr.; Lochan, R. C.; Wang, T.; Beran, G. J. O.; Besley, N. A.; Herbert, J. M.; Lin, C. Y.; Van Voorhis, T.; Chien, S. H.; Sodt, A.; Steele, R. P.; Rassolov, V. A.; Maslen, P.; Korambath, P. P.; Adamson, R. D.; Austin, B.; Baker, J.; Bird, E. F. C.; Daschel, H.; Doerksen, R. J.; Drew, A.; Dunietz, B. D.; Dutoi, A. D.; Furlani, T. R.; Gwaltney, S. R.; Heyden, A.; Hirata, S.; Hsu, C.-P.; Kedziora, G. S.; Khalliulin, R. Z.; Klunziger, P.; Lee, A. M.; Liang, W. Z.; Lotan, I.; Nair, N.; Peters, B.; Proynov, E. I.; Pieniazek, P. A.; Rhee, Y. M.; Ritchie, J.; Rosta, E.; Sherrill, C. D.; Simmonett, A. C.; Subotnik, J. E.; Woodcock, H. L., III; Zhang, W.; Bell, A. T.; Chakraborty, A. K.; Chipman, D. M.; Keil, F. J.; Warshel, A.; Herhe, W. J.; Schaefer, H. F., III; Kong, J.; Krylov, A. I.; Gill, P. M. W.; Head-Gordon, M. *Phys. Chem. Chem. Phys.* **2006**, *8*, 3172.
(45) Gauss, J.; Stanton, J. F.; Bartlett, R. J. *J. Chem. Phys.* **1991**, *95*, 2623.
(46) Koziol L. Krylov, A. I. ezVibe; http://iopenshell.usc.edu/downloads/.
(47) Bowman, J. M.; Carter, S.; Huang, X. *Int. Rev. Phys. Chem.* **2003**, *22*, 533.
(48) Jensen, P.; Bunker, P. R. *J. Chem. Phys.* **1988**, *89*, 1327.
(49) Handy, N. C., Jr.; Knowles, P. J.; Carter, S. *J. Chem. Phys.* **1991**, *94*, 118.
(50) Salem, L.; Rowland, C. *Angew. Chem., Int. Ed. Engl.* **1972**, *11*, 92.
(51) *Diradicals*; Borden, W. T., Ed.; Wiley: New York, 1982.
(52) Bonačić-Koutecký, V.; Koutecký, J.; Michl, J. *Angew. Chem., Int. Ed. Engl.* **1987**, *26*, 170.
(53) Walsh, A. D. *J. Chem. Soc.* **1953**, 2260.
(54) Hoffmann, R.; Zeiss, G. D.; Van Dine, G. W. *J. Am. Chem. Soc.* **1968**, *90*, 1485.
(55) Condon, E. *Phys. Rev.* **1926**, *28*, 1182.
(56) Duschinsky, F. *Acta Physicochim. USSR* **1937**, *7*, 551.
(57) Mozhayskiy V. A. Krylov, A. I. ezSpectrum; http://iopenshell.usc.edu/downloads/.

JP903476W